Chapter 2
Analysis of Cracked Lap Shear (CLS) Joints

Liyong Tong and Quantian Luo

Abstract This chapter presents analytical models for cracked lap shear joints. Two analytical frameworks are introduced: (1) the overlap is treated as an entire beam to find displacements and force components of the cracked lap shear joints firstly, and then the adherends in the overlap region are treated as individual beams to find adhesive stresses and energy release rates; (2) individual beams are considered only; displacements, force components and adhesive stresses are determined simultaneously by solving the coupled differential equations. Geometrically-nonlinear features of cracked lap shear joints are investigated. Strength of materials and fracture mechanics based failure criteria are discussed.

2.1 Introduction

Adhesive bonding technology has been used in aircraft structures over 70 years (Higgins 2000). In modern aeronautical and aerospace industries, this technology is widely employed to join similar and dissimilar materials to form load-bearing structural joints or integrated structures (Adams et al. 1997, Tong and Steven 1999). Adhesive bonding is especially effective to join thin metallic and/or laminated composite sheets. However, structural performance can be dramatically reduced by debonding or interface crack. It is known that debonding is mainly caused by high interface adhesive stresses, which typically exist at a free edge or terminating ends of adhesive layers and also exhibit singularity features.

Liyong Tong
School of Aerospace, Mechanical and Mechatronic Engineering, J11- Aeronautical Engineering Building, The University of Sydney, NSW 2006, Australia, e-mail: ltong@aeromech.usyd.edu.au

Quantian Luo
School of Aerospace, Mechanical and Mechatronic Engineering, J11- Aeronautical Engineering Building, The University of Sydney, NSW 2006, Australia, e-mail: qtluo@aeromech.usyd.edu.au

L.F.M. da Silva, A. Öchsner (eds.), *Modeling of Adhesively Bonded Joints*,

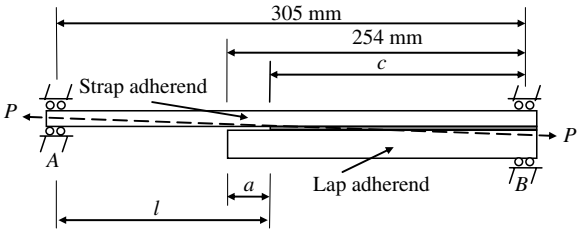

Fig. 2.1 A cracked lap shear specimen (ASTM round robin)

Due to the presence of both shear and peel stresses in an adhesive layer, fracture in adhesive or near an adhesive-adherend interface in an adhesive joint is generally a mixed-mode problem. To characterize such adhesive fracture behavior, a number of test specimens have been proposed (Mangalgiri and Johnson 1986, Rao and Acharya 1995, Alif et al. 1997). A cracked lap shear (CLS) specimen in mixed-mode condition is one of the specimens that has been widely used for characterizing fracture toughness and studying fracture behavior of adhesively bonded joints. It can also be used to simulate delamination of composite laminate and skin-flange debonding used in practical engineering structures.

An ASTM round robin (Johnson 1986) was conducted for calculating energy release rates of the CLS specimen as schematically shown in Fig. 2.1. The CLS specimen is assumed to have a width of 25 mm and a varying debond length a. In general, a CLS specimen subjected to tensile loading can have four possible combinations of support conditions at both ends (Johnson 1986, Lai et al. 1996), namely, (1) clamped-clamped, (2) roller-clamped, (3) roller-roller (similar to single lap joint), and (4) free-fixed.

One distinctive feature of the CLS is the eccentric loading path that leads to geometrical nonlinearity (Johnson 1986), and thus large deflections have to be considered in analytical and numerical analyses.

2.2 Background

The cracked lap shear specimen was firstly proposed by Brussat et al. (1977) to investigate the mixed mode fracture behavior of shear-loaded adhesive joints. The CLS have been used to study adhesive joint debonding (Brussat et al. 1977, Lin and Liechti 1987, Schmueser and Johnson 1990, Cheuk and Tong 2002) and composite delamination (Mangalgiri and Johnson 1986, Rhee 1994, Rhee and Chi 2001).

Johnson (1986) reported the ASTM round robin results conducted by nine groups or laboratories. This work was sponsored by ASTM and all participants were asked to calculate the energy release rate of the CLS specimens with four different debond lengths and two different geometries. It was indicated that, although no generally applicable closed-form solutions exist for the CLS specimen, the nonlinear finite element analysis gives the lab-to-lab consistent predictions with the observed experimental behaviors.

Analytical analysis for the CLS has attracted much attention in past several decades to sight into its essence. The analytical solutions may be obtained by modeling adherends as beams and the adhesive as a continuous spring with shear and peel stiffness. A spring model for the adhesive is widely used due to the facts that its Young's modulus is much smaller than that of the isotropic adherends, and it is normally very thin as compared to the adherends. Brussat et al. (1977), Fernlund and Spelt (1991a), Fernlund et al. (1994), and Lai et al. (1996) presented analytical analyses for the CLS specimen using the method developed by Goland and Reissner (1944) for a single lap joint. In this method, the overlap is treated as an entire beam to determine the deflections of the adhesively bonded structure and the force components at the end of the overlap as shown in Fig. 2.2.

In the light of the found CLS deflections and the overlap force components, the adhesive stresses and/or energy release rates of the interface crack can then be calculated to predict the CLS failure loads.

This method divides analysis into two steps and treats the overlap adherends as an entire or one single beam in the first step and then as two separated sub-beams in the second step (Goland and Reissner 1944). An alternative way is to combine the two steps into one and only the two separated sub-beam model for the overlap adherends is used. This coupled formulation was proposed by Hart-Smith (1973) and has been also widely used for analytical analysis of the CLS specimen. However, the overlap large deflection is not included in this coupled method. Recently, Luo and Tong (2007) presented fully coupled formulations for a single lap joint, in which adherends of the overlap are treated as two individual beams each undergoing large deflections. The adhesive stresses/energy release rates and the force components at the end of the overlap were determined simultaneously.

Experimental testing is an essential tool for validating various analyses for the CLS specimen. Not only the analytical results are required to be verified by experiments, but also the experimental test is the unique way to determine the fracture toughness of the adhesive joint to establish the fracture envelope for the CLS specimen. The experimental investigations of the CLS specimen have been conducted by a number of authors, e.g., Fernlund and Spelt (1991b), Papini et al. (1994), Wang

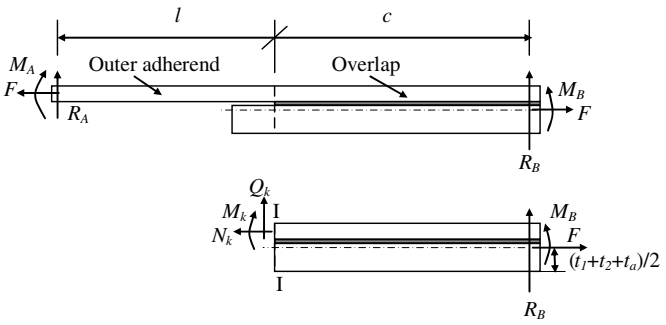

Fig. 2.2 Loadings, reaction forces and forces in cross-section I-I

et al. (1995), Benzeggaph and Kenane (1996), Rhee and Chi (2001), Rhee et al. (2003), Cheuk and Tong (2002). Both adhesive debonding and composite delamination have been tested in most of these experiments. A noticeable experimental test was conducted by Fernlund and Spelt (1994) as the fracture toughness is obtained for a full range of mode ratios.

Dattaguru et al. (1984) initially used geometrically nonlinear finite element analysis (NFEA) to numerically investigate the CLS. In the report presented by Johnson (1986), both linear and nonlinear FEA analyses were conducted. It was concluded that geometrically nonlinear FEA had to be used for the CLS specimen.

The FEA modeling of the CLS specimen may be classified into two types: a full 2D (or full 3D) model and a beam (or plate) model with adhesive elements. In the full 2D (or full 3D) model, 2D (or 3D) elements are used to model both adherends and adhesive. A full 3D FEA is an effective tool for the CLS specimen. However, it is well known that it can be computationally expensive and may even encounter numerical difficulty for beam-type and plate/shell-type structures. As concerned about a beam model with adhesive elements, Carpenter (1973, 1980) developed a constant shear and extensional spring element for adhesive idealization. Kuo (1984) developed a continuous spring element with shear stiffness. Luo and Tong (2004) derived a continuous spring element with shear and peel stiffness. These two types of FEA models for adhesive joints can also be combined. Ko et al. (1994) used the weighted adhesive plate element for the CLS specimen, Wu and Crocombe (1996) used beam elements to model the adherends and 2D elements to depict the adhesive.

With the development of commercial FEA software, full 2D (or full 3D) models have been widely used (Wu and Crocombe 1996, Cheuk and Tong 2002, Yang et al. 2003, Luo and Tong 2007). When NFEA is used for the CLS analysis, energy release rates (ERR) and/or stress intensity factors are required to be calculated when the fracture mechanics based failure criteria are used. In this case, virtual crack closure technique (VCCT) (Harbert and Hogan 1992, Rhee and Ernst 1993, Panigrahi and Pradhan 2007, Yang et al. 2007) has been widely used.

2.3 Fundamental Formulations

In this section, the fundamentals of analytical solutions for the CLS specimen will be discussed. Two theoretical frameworks mentioned in Sect. 2.2 will be discussed in details: (1) the CLS deflections and the force components at the overlap end are determined firstly and then the adhesive stresses and/or energy release rates (ERRs) are calculated, and (2) the CLS displacements, the overlap forces and the adhesive stresses/ERRs are determined simultaneously.

In the first analytical framework, analytical analysis for the cracked lap shear consists of two parts: (1) find deflections of the CLS specimen and the force components at the overlap end by taking into account large deflections as shown in Fig. 2.2, and (2) stress analysis and/or ERR calculation for failure prediction.

The force components at the overlap end include the applied force F, reaction force R_B and moment M_B and forces in cross-section I-I: axial force N_k, shear force V_k (or Q_k) and bending moment M_k, where V_k is the transverse shear force perpendicular to the deformed beam axis and Q_k is that perpendicular to the un-deformed beam axis. The key force component is the edge bending moment M_k at the overlap end as the other components of cross-section I-I may be found by the equilibrium equations or the differential relations of internal forces based on the beam theory. The bending moment at the adhesive edge can be defined as:

$$M_k = kF\left(\frac{t_2 + t_a}{2}\right) \tag{2.1}$$

where k is the edge moment factor; t_2 and t_a are thicknesses of the lap adherend and the adhesive. It is noted that $(t_2 + t_a/2)$ is the distance of two horizontal forces (see Fig. 2.2), and when $t_1 = t_2 = t$, definitions of the edge moment and its factor in Eq. (2.1) are consistent with those of Goland and Reissner (1944) for a single lap joint.

The edge moment of a cracked lap shear specimen can be found on the basis of the method proposed by Goland and Reissner (1944), who treated the overlap as an entire Euler beam. In the light of this model, Fernlund et al. (1994) determined the edge moment and the CLS deflections for calculating the value of J-integral. Lai et al. (1996) also used this method to find the overlap force components and then calculated the ERRs for the CLS specimen.

After determining the CLS deflections and the overlap force components, the adhesive stresses can be solved based on the formulations developed by Goland and Reissner (1994), and the energy release rates can be calculated by using the J-integration with the mode partition (Fernlund and Spelt 1991a, Fernlund et al. 1994) and the interface crack theory (Suo and Hutchinson 1990, Lai et al. 1996).

In the second analytical framework, fully-coupled equations are treated. The edge moment, displacements and the adhesive stresses were solved at the same time. This framework has been used to analyze the CLS with the roller-roller boundary condition (SLJ) by Hart-Smith (1973), Oplinger (1994), and Luo and Tong (2007). In the Hart-Smith model (1973), large deflections of the overlap were not considered. In the Oplinger's model (1994), large deflections of the overlap coupled with the adhesive shear stress but not peel stress were considered. Luo and Tong (2007) considered large deflections with coupled both shear and peel stresses. The formulation of the second framework can also be extended to the CLS with the other boundary conditions using the same procedure.

2.3.1 Basic Equations for the Outer Adherend and Reaction Forces

To find the CLS displacements and the overlap force components, we need to consider the equilibrium, constitutive and continuity conditions of the CLS specimen.

The free body diagrams of the CLS specimen and the overlap are shown in Fig. 2.2. The applied force F is the horizontal component of load P. The equilibrium equations of the CLS specimen are:

$$R_B + R_A = 0 \tag{2.2}$$

$$M_B - M_A + F\left(\frac{t_2 + t_a}{2}\right) - R_A(l + c) = 0 \tag{2.3}$$

In the first framework, deflections of the CLS specimen are schematically illustrated in Fig. 2.3. The bending moment of the outer adherend and the overlap is respectively:

$$M_3(x_3) = -Fw_3 + R_A x_3 + M_A \qquad 0 \le x_3 \le l \tag{2.4}$$

$$M_o(x_o) = -Fw_o - R_B x_o + M_B \qquad -c \le x_o \le 0 \tag{2.5}$$

The constitutive relations of the outer adherend and the overlap based on the Euler beam are:

$$M_3 = -D_{11}\frac{d^2 w_3}{dx_3^2}; \quad M_o = -D_o\frac{d^2 w_o}{dx_o^2} \tag{2.6}$$

where D_{11} and D_o are bending stiffness of the outer adherend and the overlap. Substituting Eq. (2.6) into Eqs. (2.4) and (2.5) yields:

$$w_3 = A_1 \sinh\beta_k x_3 + A_2 \cosh\beta_k x_3 + \frac{R_A}{F}x_3 + \frac{M_A}{F} \tag{2.7}$$

$$w_o = B_1 \sinh\beta_o x_o + B_2 \cosh\beta_o x_o - \frac{R_B}{F}x_o + \frac{M_B}{F} \tag{2.8}$$

In Eqs. (2.7) and (2.8), A_1, A_2, B_1 and B_2 are the unknown integration constants, which are to be determined by using the relevant boundary conditions; and the eigenvalues are:

$$\beta_k = \sqrt{\frac{F}{D_{11}}}; \quad \beta_o = \sqrt{\frac{F}{D_o}} \tag{2.9}$$

It is noted that, in Eqs. (2.7) and (2.8), there are 4 integration constants and 4 reaction force components to be determined. To find the 8 unknowns, we need to have 8 independent equations. By the support conditions at A and B, 4 boundary

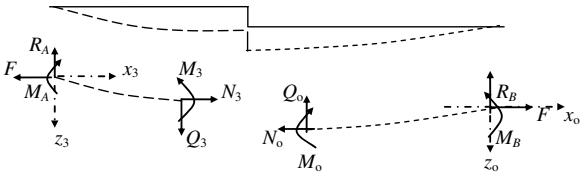

Fig. 2.3 Deflections and coordinate systems of the CLS specimen

equations can be derived; 2 equilibrium equations are given in Eqs. (2.2) and (2.3); the other 2 equations are obtained by the continuity conditions at cross-section I-I.

The continuity conditions at cross section I-I can be written as:

$$u_3(l) = u_o(-c); \quad w_3(l) = w_o(-c); \frac{dw_3(l)}{dx_3} = \frac{dw_o(-c)}{dx_o} \tag{2.10}$$

Equation (2.10) is the general requirements of deformation continuity; the axial continuity condition was not used for the formulation based on the method of Goland and Reissner (1944).

The 4 integration constants and the 4 unknowns R_A, M_A, R_B and M_B can be found by the 4 boundary condition equations that will be discussed in Subsection 2.3.3 and the 4 equations given in Eqs. (2.2), (2.3) and (2.10). Therefore, the CLS deflections are solved and then the edge moment M_k the edge shear force V_k are found by:

$$M_k = -D_{11}\frac{d^2w_3(l)}{dx_3^2}; \quad V_k = \frac{dM_3(l)}{dx_3} \tag{2.11}$$

When the CLS deflections and force components of the overlap are solved, adhesive stresses and the ERRs can then be found.

2.3.2 Basic Equations for the Overlap and Adhesive Stresses

When upper and lower adherends are identical, or symmetrical adherends, solutions of the shear and peel stresses for the prescribed force boundary conditions of the overlap were presented by Goland and Reissner (1944). For the asymmetrical adherends, solutions of the adhesive stresses can be found in Luo and Tong (2002). In this chapter, we only present adhesive stress analysis for the symmetrical adherends and introduce the following variables:

$$\begin{cases} 2u_s = u_2 + u_1; \quad 2w_s = w_2 - w_1; \quad 2u_a = u_2 - u_1; \quad 2w_a = w_2 + w_1 \\ 2N_s = N_2 + N_1; \quad 2Q_s = Q_2 - Q_1; \quad 2M_s = M_2 - M_1 \\ 2N_a = N_2 - N_1; \quad 2Q_a = Q_2 + Q_1; \quad 2M_a = M_2 + M_1 \end{cases} \tag{2.12}$$

The variables in Eq. (2.12) have the usual meanings used in the Euler beam theory; subscripts 1 and 2 refer to identical adherends 1 and 2 in the overlap region; the force components are shown in the free body diagrams of the infinitesimal elements, see Fig. 2.4.

The equilibrium equations of adherends 1 and 2 in the overlap can be derived from Fig. 2.4, as:

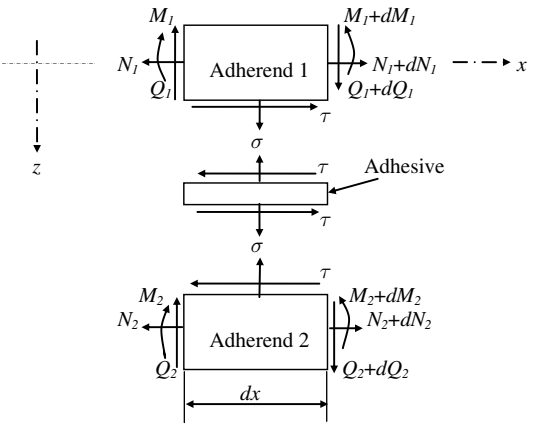

Fig. 2.4 Free body diagram for stress analysis of adhesive joints

$$\begin{cases} \dfrac{dN_1}{dx}+\tau=0; \quad \dfrac{dQ_1}{dx}+\sigma=0; \quad \dfrac{dM_1}{dx}+\dfrac{t_1}{2}\tau-Q_1=0 \\ \dfrac{dN_2}{dx}-\tau=0; \quad \dfrac{dQ_2}{dx}-\sigma=0; \quad \dfrac{dM_2}{dx}+\dfrac{t_1}{2}\tau-Q_2=0 \end{cases} \tag{2.13}$$

In Eq. (2.13), τ and σ are the adhesive shear and peel stresses, whose definitions are given by Goland and Reissner (1944):

$$\tau=\frac{G_a}{t_a}\left[(u_2-u_1)+\frac{t_1}{2}\left(\frac{dw_1}{dx}+\frac{dw_2}{dx}\right)\right]; \quad \sigma=\frac{E_a(w_2-w_1)}{t_a} \tag{2.14}$$

In Eq. (2.14), E_a and G_a are Young's and shear moduli of the adhesive. By making use of the variables in Eq. (2.12), Eqs. (2.13) and (2.14) become:

$$\begin{cases} \dfrac{dN_s}{dx}=0; \quad \dfrac{dQ_s}{dx}-\sigma=0; \quad \dfrac{dM_s}{dx}-Q_s=0 \\ \dfrac{dN_a}{dx}-\tau=0; \quad \dfrac{dQ_a}{dx}=0; \quad \dfrac{dM_a}{dx}+\dfrac{t_1}{2}\tau-Q_a=0 \end{cases} \tag{2.15}$$

$$\tau=\frac{2G_a}{t_a}\left(u_a+\frac{t_1}{2}\frac{dw_a}{dx}\right); \quad \sigma=\frac{2E_a w_s}{t_a} \tag{2.16}$$

The constitutive relations of the Euler beam are:

$$N=A_{11}\frac{du}{dx}; \quad M=-D_{11}\frac{d^2w}{dx^2} \tag{2.17}$$

where A_{11} is the extensional stiffness of the adherends.

It is noted that shear and peel stresses have been decoupled in Eq. (2.15), in which, the 1st and the 2nd row of equations can be used to solve the peel stress and

shear stress respectively. By substituting Eq. (2.17) into (2.15), and then substituting u_a, w_a and w_s into Eq. (2.16), the governing differential equations for the shear and peel stresses can be obtained as follows:

$$\frac{d^3\tau}{dx^3} - \frac{2G_a}{A_{11}t_a}\left(1+\frac{A_{11}t_1^2}{4D_{11}}\right)\frac{d\tau}{dx} = 0; \quad \frac{d^4\sigma}{dx^4} + \frac{2E_a}{D_{11}t_a}\sigma = 0 \tag{2.18}$$

The analytical solutions of Eqs. (2.18) are:

$$\begin{cases} \tau = A_1\sinh\beta_a x + A_2\cosh\beta_a x + A_3 \\ \sigma = B_1\sinh\beta_\sigma x\sin\beta_\sigma x + B_2\sinh\beta_\sigma x\cos\beta_\sigma x \\ \qquad + B_3\cosh\beta_\sigma x\sin\beta_\sigma x + B_4\cosh\beta_\sigma x\cos\beta_\sigma x \end{cases} \tag{2.19}$$

In Eq. (2.19), $A_i (i = 1, 2, 3)$ and $B_j (j = 1, 2, 3, 4)$ are the integration constants, and the eigenvalues are:

$$\begin{cases} \beta_a^2 = \alpha_a\beta_\tau^2; \quad \beta_\tau = \sqrt{\dfrac{8G_a}{A_{11}t_a}}; \quad \beta_\sigma = \dfrac{\sqrt{2}}{2}\sqrt[4]{\dfrac{2E_a}{D_{11}t_a}} \\ \alpha_a = \dfrac{(1+\alpha_k)}{4}; \quad \alpha_k = \dfrac{A_{11}t_1^2}{4D_{11}} \end{cases} \tag{2.20}$$

where coefficients α_a and α_k may reflect influence of the lay-up sequence when the overlap adherends are composite laminates with the symmetrical lay-up. For the isotropic adherends, $\alpha_a = 1$ and $\alpha_k = 3$.

The integration constants in Eq. (2.19) can be determined by the prescribed force boundary conditions of the overlap, and the force components of the overlap are dependent on loadings, support conditions and geometrical configurations of the CLS specimen.

In this analytical method, large deflections are considered to find the force components of the overlap but not for the adhesive stresses. The entire beam model and the sub-beam model are applied to the overlap force determination and the adhesive stress analysis respectively.

Hart-Smith (1973) presented the coupled formulations for a single lap joint. By substituting Eqs. (2.16) and (2.17) into Eq. (2.15), the governing differential equations for adherend displacements can be obtained:

$$\frac{d^2u_s}{dx^2} = 0; \quad D_{11}\frac{d^4w_s}{dx^4} + \frac{2E_a}{t_a}w_s = 0 \tag{2.21}$$

$$\begin{cases} \dfrac{d^2u_a}{dx^2} - \dfrac{2G_a}{A_{11}t_a}\left(u_a + \dfrac{t_1}{2}\dfrac{dw_a}{dx}\right) = 0 \\ -\dfrac{d^4w_a}{dx^4} + \dfrac{G_at_1}{D_{11}t_a}\left(\dfrac{du_a}{dx} + \dfrac{t_1}{2}\dfrac{d^2w_a}{dx^2}\right) = 0 \end{cases} \tag{2.22}$$

Equations (2.21) and (2.22) can be analytically solved, whose integration constants are solved by boundary conditions of the overlap. The solved integration constants include unknowns: edge bending moment M_k and rigid body motions. These unknowns should be solved by the continuity conditions at I-I and support conditions of the CLS specimen. It is noted that all the 3 continuity equations given in Eq. (2.10) will be used in this coupled formulations. To use the continuity condition with respect to the axial deformation, the axial displacement of the outer adherend needs to be used. It can be solved by referring to Fig. 2.3 and the constitutive relations, which are given by:

$$u_3 = \frac{F}{A_{11}} x_3 + C_1 \tag{2.23}$$

where C_1 is the integration constant.

Because large deflections of the overlap are not included in adhesive stress analysis presented in Eq. (2.13) and the solutions given in Eq. (2.19), the analytical solutions of Hart-Smith (1973) do not model the overlap large deflection.

By analyzing the Goland and Reissner's formulation (1944) and the Hart-Smith's one (1973), the former considered large deflections of the overlap but ignored adhesive deformation, whereas the latter considered shear and peel strains but neglect the overlap large deflections.

Recently, Luo and Tong (2007) presented the fully-coupled nonlinear analysis for SLJs, in which, both large deflections and adhesive deformations are modeled. In this method, equilibrium equations of the infinitesimal adherend elements are derived on the basis of the geometrically nonlinear analysis. As shown in Fig. 2.5, the equilibrium equations for the free body diagrams are:

$$\begin{cases} dN_1 + \tau(ds_1)\dfrac{dx}{ds_1} = 0; \quad dQ_1 + \sigma(dx) + \tau\dfrac{dw_1}{dx}dx = 0 \\ dM_1 + \dfrac{t_1}{2}\tau(dx) - Q_1 dx = -N_1\dfrac{dw_1}{dx}dx \\ dN_2 - \tau(ds_2)\dfrac{dx}{ds_2} = 0; \quad dQ_2 - \sigma(dx) - \tau\dfrac{dw_2}{dx}dx = 0 \\ dM_2 + \dfrac{t_1}{2}\tau(dx) - Q_2 dx = -N_2\dfrac{dw_2}{dx}dx \end{cases} \tag{2.24}$$

where, $(ds_1)^2 = (dx)^2 + (dw_1)^2$ and $(ds_2)^2 = (dx)^2 + (dw_2)^2$.

By using the variables in Eq. (2.12), the equilibrium equations become:

$$\begin{cases} \dfrac{dN_s}{dx} = 0 \\ \dfrac{dQ_s}{dx} - \sigma - \tau\dfrac{dw_a}{dx} = 0; \quad \dfrac{dM_s}{dx} - Q_s = -N_s\dfrac{dw_s}{dx} - N_a\dfrac{dw_a}{dx} \end{cases} \tag{2.25}$$

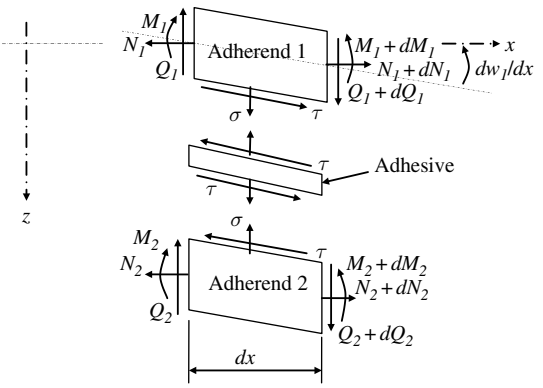

Fig. 2.5 Free body diagram for nonlinear analysis of adhesive joints

$$\begin{cases} \dfrac{dN_a}{dx} - \tau = 0 \\ \dfrac{dQ_a}{dx} - \tau\dfrac{dw_s}{dx} = 0; \quad \dfrac{dM_a}{dx} + \dfrac{t_1}{2}\tau - Q_a = -N_s\dfrac{dw_a}{dx} - N_a\dfrac{dw_s}{dx} \end{cases} \tag{2.26}$$

The nonlinear constitutive relations of the Euler beam are:

$$\begin{cases} N = A_{11}\left[\dfrac{du}{dx} + \dfrac{1}{2}\left(\dfrac{du}{dx}\right)^2 + \dfrac{1}{2}\left(\dfrac{dw}{dx}\right)^2\right] - B_{11}\dfrac{d^2w}{dx^2} \\ M = B_{11}\left[\dfrac{du}{dx} + \dfrac{1}{2}\left(\dfrac{du}{dx}\right)^2 + \dfrac{1}{2}\left(\dfrac{dw}{dx}\right)^2\right] - D_{11}\dfrac{d^2w}{dx^2} \end{cases} \tag{2.27}$$

where the coupling extension and bending stiffness B_{11} is equal to zero for the symmetrical cross section. In Eqs. (2.16) and (2.25), (2.26), (2.27), 12 equations consists of 12 variables: 6 stress resultants and 4 adherend displacements plus shear and peel stresses.

In Eqs. (2.25) and (2.26), differentiating the bending moment equilibrium equations, into which, substituting the shear force equations, and utilizing the axial force equilibrium equations, we have:

$$\frac{d^2M_s}{dx^2} - \sigma = -N_s\frac{d^2w_s}{dx^2} - N_a\frac{d^2w_a}{dx^2} \tag{2.28}$$

$$\frac{d^2M_a}{dx^2} + \frac{t_1}{2}\frac{d\tau}{dx} = -N_s\frac{d^2w_a}{dx^2} - N_a\frac{d^2w_s}{dx^2} \tag{2.29}$$

When the following higher order nonlinear terms are ignored:

$$\frac{du_a}{dx}\frac{d^2w_s}{dx^2} \quad \frac{du_a}{dx}\frac{d^2w_a}{dx^2} \tag{2.30}$$

The simplified equilibrium equations including effects of the overlap large deflections can be obtained:

$$\frac{dN_s}{dx}=0; \quad \frac{d^2M_s}{dx^2}-\sigma=-\frac{F}{2}\frac{d^2w_s}{dx^2} \tag{2.31}$$

$$\frac{dN_a}{dx}-\tau=0; \quad \frac{d^2M_a}{dx^2}+\frac{t_1}{2}\frac{d\tau}{dx}=-\frac{F}{2}\frac{d^2w_a}{dx^2} \tag{2.32}$$

In Eqs. (2.31) and (2.32), the relation $N_s=(N_1+N_2)/2=F/2$ has been used. In the definitions of adhesive shear and peel strains of Eq. (2.14), small strains and rotations of the adherends are assumed. By using this assumption, higher order terms in Eq. (2.27) can be neglected. Utilizing Eq. (2.12), we have:

$$N_i=A_{11}\frac{du_i}{dx} \qquad M_i=-D_{11}\frac{d^2w_i}{dx^2} \qquad (i=s,a) \tag{2.33}$$

By substituting Eqs. (2.16) and (2.33) into Eqs. (2.31) and (2.32), the following governing equations in terms of displacements of adherends in the overlap region of the CLS specimen can be obtained:

$$\begin{cases} \dfrac{d^2u_s}{dx^2}=0; \\ D_{11}\dfrac{d^4w_s}{dx^4}-\dfrac{F}{2}\dfrac{d^2w_s}{dx^2}+\dfrac{2E_a}{t_a}w_s=0 \end{cases} \tag{2.34}$$

$$\begin{cases} A_{11}\dfrac{d^2u_a}{dx^2}-\dfrac{2G_a}{t_a}\left(u_a+\dfrac{t_1}{2}\dfrac{dw_a}{dx}\right)=0 \\ -D_{11}\dfrac{d^4w_a}{dx^4}+\dfrac{G_at_1}{t_a}\left(\dfrac{du_a}{dx}+\dfrac{t_1}{2}\dfrac{d^2w_a}{dx^2}\right)+\dfrac{F}{2}\dfrac{d^2w_a}{dx^2}=0 \end{cases} \tag{2.35}$$

From a mathematical viewpoint, Eqs. (2.34) and (3.35) are linear differential equations for the given axial load F, and can be analytically solved. The closed-form solutions of Eqs. (3.34) and (3.35) are (Luo and Tong 2008):

$$\begin{cases} u_s=A_{s1}x+A_{s2} \\ w_s=(B_{s1}\sinh\beta_{s1}x+B_{s2}\cosh\beta_{s1}x)\sin\beta_{s2}x \\ \qquad +(B_{s3}\sinh\beta_{s1}x+B_{s4}\cosh\beta_{s1}x)\cos\beta_{s2}x \end{cases} \tag{2.36}$$

$$\begin{cases} u_a=A_{a1}\sinh\beta_{a1}x+A_{a2}\cosh\beta_{a1}x \\ \qquad +A_{a3}\sinh\beta_{a2}x+A_{a4}\cosh\beta_{a2}x+A_{a5} \\ w_a=B_{a1}\sinh\beta_{a1}x+B_{a2}\cosh\beta_{a1}x \\ \qquad +B_{a3}\sinh\beta_{a2}x+B_{a4}\cosh\beta_{a1}x+B_{a5}x+B_{a6} \end{cases} \tag{2.37}$$

where, A_{s1}, A_{s2}, B_{si} ($i = 1, 2, 3, 4$), A_{a1} and B_{aj} ($i = 1, 2, \cdots, 5$; $j = 1, 2, \cdots, 6$) are the integration constants, which are determined by the boundary conditions. The eigenvalues are respectively (Luo and Tong 2008):

$$\beta_{s1} = \sqrt{\beta_\sigma^2 + \frac{\beta_k^2}{8}}, \quad \beta_{s2} = \sqrt{\beta_\sigma^2 - \frac{\beta_k^2}{8}} \tag{2.38}$$

$$\begin{cases} \beta_{a1}^2 = \dfrac{1}{2}\left[\alpha_a\beta_\tau^2 + \dfrac{\beta_k^2}{2} + \sqrt{\alpha_a^2\beta_\tau^4 + (\alpha_a - \dfrac{1}{2})\beta_\tau^2\ \beta_k^2 + \dfrac{\beta_k^4}{4}}\right] \\ \beta_{a2}^2 = \dfrac{1}{2}\left[\alpha_a\beta_\tau^2 + \dfrac{\beta_k^2}{2} - \sqrt{\alpha_a^2\beta_\tau^4 + (\alpha_a - \dfrac{1}{2})\beta_\tau^2\ \beta_k^2 + \dfrac{\beta_k^4}{4}}\right] \end{cases} \tag{2.39}$$

For the case of isotropic adherends, Eq. (2.39) degenerates:

$$\begin{cases} \beta_{a1}^2 = \dfrac{1}{2}\left(\beta_\tau^2 + \dfrac{\beta_k^2}{2} + \sqrt{\beta_\tau^4 + \dfrac{\beta_\tau^2\beta_k^2}{2} + \dfrac{\beta_k^4}{4}}\right) \\ \beta_{a2}^2 = \dfrac{1}{2}\left(\beta_\tau^2 + \dfrac{\beta_k^2}{2} - \sqrt{\beta_\tau^4 + \dfrac{\beta_\tau^2\beta_k^2}{2} + \dfrac{\beta_k^4}{4}}\right) \end{cases} \tag{2.39a}$$

By using the overlap boundary conditions, the integration constants with the unknowns of the edge moment and the rigid body motions can be solved. The unknowns can be solved by the continuity conditions in Eq. (2.10) and the support conditions.

It can be seen that, in the second analytical framework of the coupled nonlinear analysis, large deflections of the outer adherend and the overlap, and the adhesive deformations have been considered. The CLS displacements, force components and adhesive stresses can be simultaneously solved.

2.3.3 Boundary Conditions, Loading Cases and Analytical Solution

2.3.3.1 Boundary Conditions

To analytically solve the CLS for the 4 possible boundary conditions of the CLS, we first derive the boundary equations in terms of the displacements (Johnson 1986, Lai et al. 1996):

(1) Clamped-Clamped

$$w_3(0) = 0; \quad \frac{dw_3(0)}{dx_3} = 0 \text{ and } w_o(0) = 0; \ \frac{dw_o(0)}{dx_o} = 0 \tag{2.40}$$

(2) Roller-Clamped

$$w_3(0) = 0; \quad M_A = 0 \text{ and } w_o(0) = 0; \ \frac{dw_o(0)}{dx_o} = 0 \tag{2.41}$$

(3) Roller-Roller (equivalent to single lap joint)

$$w_3(0) = 0; \quad M_A = 0 \text{ and } w_o(0) = 0; \ M_B = 0 \text{ or } \frac{d^2w_o(0)}{dx_o^2} = 0 \tag{2.42}$$

(4) Free-Fixed

$$M_A = 0; \quad R_A = 0 \text{ and } w_o(0) = 0; \ \frac{dw_o(0)}{dx_o} = 0 \tag{2.43}$$

2.3.3.2 Loading Cases

The CLS specimen is subjected to a pair of tensile forces (P) in the experimental test, as shown in Fig. 2.1. The axial force F in Fig. 2.2 is the project of P in the horizontal direction, which is given by:

$$F = \frac{(l+c)P}{\sqrt{(l+c)^2 + [(t_2+t_a)/2]^2}} \tag{2.44}$$

The loading cases for the CLS testing specimen are illustrated in Fig. 2.2. In this chapter, we present analytical analysis for the CLS specimen subjected to the tensile force only. For engineering structures with lap shear joints, they may be subjected to transverse forces and bending moments, whose solutions can be found using the similar procedure.

2.3.3.3 The 1st Step Solutions of the 1st Analytical Framework

In the 1st analytical framework, solution procedures of the 1st step are to determine the 8 unknowns in Eqs. (2.7) and (2.8) using the 8 equations given in Eqs. (2.2), (2.3), (2.10) and (2.40) or (2.41) or (2.42) or (2.43). Lai et al. (1996) derived force components of the overlap for the boundary conditions of Clamped-Clamped and Roller-Clamped. Goland and Reissner (1944) derived the edge moment for the Roller-Roller boundary conditions and the symmetrical substrates. The consistent formulations for the general CLS with the 4 possible boundary conditions are presented below.

(1) Clamped-Clamped:
Substituting Eq. (2.40) into Eqs. (2.7) and (2.8) and combining Eqs. (2.2) and (2.3), we have:

$$\begin{cases} A_2 + \dfrac{M_A}{F} = 0;\ \beta_k A_1 + \dfrac{R_A}{F} = 0;\ B_2 + \dfrac{M_B}{F} = 0;\ \beta_o B_1 - \dfrac{R_B}{F} = 0 \\ B_1 = \dfrac{\beta_k}{\beta_o} A_1;\ B_2 = A_2 + A_1 \beta_k (l+c) + \dfrac{t_2 + t_a}{2} \end{cases} \tag{2.45}$$

By utilizing Eq. (2.45), Eqs. (2.7) and (2.8) become:

$$w_3 = A_1 (\sinh \beta_k x_3 - \beta_k x_3) + A_2 (\cosh \beta_k x_3 - 1) \tag{2.46}$$

$$\begin{aligned} w_o = {} & A_1 \left[\frac{\beta_k}{\beta_o} (\sinh \beta_o x_o - \beta_o x_o) + \beta_k (l+c) (\cosh \beta_o x_o - 1) \right] \\ & + A_2 (\cosh \beta_o x_o - 1) + \frac{t_2 + t_a}{2} (\cosh \beta_o x_o - 1) \end{aligned} \tag{2.47}$$

By substituting Eqs. (2.46) and (2.47) into Eq. (2.10), the following algebraic equations can be obtained:

$$\begin{cases} A_1 [\beta_k \beta_o (l+c) \cosh \beta_o c - \beta_k \sinh \beta_o c - \beta_o \sinh \beta_k l] \\ \quad + A_2 \beta_o (\cosh \beta_o c - \cosh \beta_k l) = \frac{t_2 + t_a}{2} \beta_o (\cosh \beta_o c - 1) \\ A_1 [\beta_k (\cosh \beta_o c - \cosh \beta_k l) - \beta_k (l+c) \sinh \beta_o c] \\ \quad - A_2 (\beta_k \sinh \beta_k l + \beta_o \sinh \beta_o c) = \frac{t_2 + t_a}{2} \beta_o \sinh \beta_o c \end{cases} \tag{2.48}$$

The integration constants A_1 and A_2 are readily solved from Eq. (2.48), and then B_1, B_2, R_A, R_B, M_A and M_B are obtained by Eq. (2.45). Since deflections and reaction force components are determined, the edge moment is found from Eq. (2.11)

(2) Roller-Clamped:
Substituting Eq. (2.41) into Eqs. (2.2), (2.3), (2.7) and (2.8) yields:

$$\begin{cases} A_2 = 0;\ B_2 + \dfrac{M_B}{F} = 0;\ \dfrac{R_B}{F} = -\dfrac{R_A}{F} = \beta_o B_1 \\ \dfrac{M_B}{F} = -\beta_o B_1 (l+c) - \dfrac{t_2 + t_a}{2} \end{cases} \tag{2.49}$$

Substituting Eq. (2.49) into Eqs. (2.7) and (2.8), we have:

$$w_3 = A_1 \sinh \beta_k x_3 - \beta_o B_1 x_3 \tag{2.50}$$

$$\begin{aligned} w_o = {} & B_1 [(\sinh \beta_o x_0 - \beta_o x_o) + \beta_k (l+c) (\cosh \beta_o x_o - 1)] \\ & + \frac{t_2 + t_a}{2} (\cosh \beta_o x_o - 1) \end{aligned} \tag{2.51}$$

A set of equations used to determine the integration constants can be obtained by substituting Eqs. (2.50) and (2.51) into Eq. (2.10):

$$\begin{cases} A_1\beta_k\cosh\beta_k l + B_1\beta_o\left[\beta_o\left(l+c\right)\sinh\beta_o c - \cosh\beta_o c\right] = -\dfrac{t_2+t_a}{2}\beta_o\sinh\beta_o c \\ A_1\sinh\beta_k l + B_1\left[\sinh\beta_o c - \beta_o\left(l+c\right)\cosh\beta_o c\right] = \dfrac{t_2+t_a}{2}\left(\cosh\beta_o c - 1\right) \end{cases} \tag{2.52}$$

By solving Eq. (2.52), the integration constants A_1 and B_1 are determined and then B_2, R_A, R_B and M_B are obtained by Eq. (2.49). The deflections and reaction forces for the CLS are determined.

(3) Roller-Roller:
Substituting Eq. (2.42) into Eqs. (2.2), (2.3), (2.7) and (2.8), we have:

$$R_A = -R_B = \alpha F;\ A_2 = 0;\ B_2 = 0 \qquad \text{where, } \alpha = \frac{t_2+t_a}{2(l+c)} \tag{2.53}$$

Equations (2.7) and (2.8) become:

$$w_3 = A_1\sinh\beta_k x_3 + \alpha\cdot x_3 \tag{2.54}$$

$$w_o = B_1\sinh\beta_o x_o + \alpha\cdot x_o \tag{2.55}$$

By substituting Eqs. (2.54) and (2.55) into Eq. (2.10), the integration constants A_1 and B_1 are obtained:

$$\begin{cases} A_1 = -\dfrac{\beta_o\left(t_2+t_a\right)\cosh\beta_o c}{2\left(\beta_o\sinh\beta_k l\cosh\beta_o c + \beta_k\cosh\beta_k l\sinh\beta_o c\right)} \\ B_1 = -\dfrac{\beta_k\left(t_2+t_a\right)\cosh\beta_k l}{2\left(\beta_o\sinh\beta_k l\cosh\beta_o c + \beta_k\cosh\beta_k l\sinh\beta_o c\right)} \end{cases} \tag{2.56}$$

The edge moment can be found from Eqs. (2.11), (2.54) and (2.56), and the edge moment factor is given by:

$$k = \frac{1}{1+\dfrac{\beta_k}{\beta_o}\tanh\beta_o c\coth\beta_k l} = \frac{1}{1+\sqrt{\dfrac{D_o}{D_{11}}}\tanh\sqrt{\dfrac{D_{11}}{D_o}}\beta_k c\coth\beta_k l} \tag{2.57}$$

When $t_1 = t_2 = t$ and $t_a << t$ (i.e., $D_0 = 8D_{11}$), Eq. (2.57) becomes:

$$k = \frac{1}{1+2\sqrt{2}\tanh\left(\dfrac{\beta_k c}{2\sqrt{2}}\right)\coth\beta_k l} \tag{2.58}$$

Equation (2.58) was recovered from the formulations of Goland and Reissner (1944) by Tsai and Morton (1994). It is noted that the edge moment factor given by Goland and Reissner (1944) is the simplified one for the long outer adherend ($\beta_k l >> 1$).

(4) Free-Fixed:
Combining Eq. (2.43) with Eqs. (2.2), (2.3), (2.7), (2.8), we have:

$$R_B = 0;\ M_B = -F\left(\frac{t_2+t_a}{2}\right);\ B_1 = 0;\ B_2 = \frac{t_2+t_a}{2} \tag{2.59}$$

Equations (2.7) and (2.8) become:

$$w_3 = A_1 \sinh\beta_k x_3 + A_2 \cosh\beta_k x_3 \tag{2.60}$$

$$w_o = \frac{t_2+t_a}{2}(\cosh\beta_o x_o - 1) \tag{2.61}$$

The integration constants A_1 and A_2 are readily determined By Eqs. (2.10), (2.60) and (2.61):

$$\begin{cases} A_1 = -\dfrac{t_2+t_a}{2}\left[\sinh\beta_k l\,(\cosh\beta_o c - 1) + \dfrac{\beta_o}{\beta_k}\cosh\beta_k l \sinh\beta_o c\right] \\ A_2 = \dfrac{t_2+t_a}{2}\left[\cosh\beta_k l\,(\cosh\beta_o c - 1) + \dfrac{\beta_o}{\beta_k}\sinh\beta_k l \sinh\beta_o c\right] \end{cases} \tag{2.62}$$

The edge moment factor is:

$$k = -\left(\cosh\sqrt{\frac{D_{11}}{D_0}}\beta_k c - 1\right) \tag{2.63}$$

2.3.3.4 Adhesive Stresses

When the CLS deflections and the overlap force components are solved, the adhesive stresses and the energy release rates (ERR) can be calculated. The ERR calculations will be discussed in Sect. 2.5.

The large deflections of the overlap are not included for the adhesive stress analysis in the 1st analytical framework based on the method of Goland and Reissner (1944) and the 2nd formulation framework based on the approach of Hart-Smith (1973). For the prescribed force boundary conditions, the same adhesive stresses are obtained based on the formulations of Goland and Reissner (1944) and Hart-Smith (1973). For the symmetrical CLS with the roller-roller boundary conditions, shear and peel stresses are:

$$\begin{cases} \tau = \dfrac{\beta_\tau(Ft_1 + 6M_k)\cosh\beta_\tau x}{8t_1 \sinh\beta_\tau c} + \dfrac{3(Ft_1 - 2M_k)}{8t_1 c} \\ \sigma = \dfrac{2\beta_\sigma^2\,(B_{\sigma 1}\sinh\beta_\sigma x \sin\beta_\sigma x + B_{\sigma 4}\cosh\beta_\sigma x \cos\beta_\sigma x)}{\sinh 2\beta_\sigma c + \sin 2\beta_\sigma c} \end{cases} \tag{2.64}$$

where,

$$\begin{cases} B_{\sigma 1} = M_k(\sinh\beta_\sigma c\cos\beta_\sigma c + \cosh\beta_\sigma c\sin\beta_\sigma c) + \dfrac{V_k}{\beta_\sigma}\sinh\beta_\sigma c\sin\beta_\sigma c \\ B_{\sigma 4} = M_k(\sinh\beta_\sigma c\cos\beta_\sigma c - \cosh\beta_\sigma c\sin\beta_\sigma c) + \dfrac{V_k}{\beta_\sigma}\cosh\beta_\sigma c\cos\beta_\sigma c \end{cases} \tag{2.65}$$

The maximum shear and peel stresses are:

$$\begin{cases} \tau_{\max} = \dfrac{1}{8}\left[(3k_1+1)\beta_\tau\coth\beta_\tau c + 3(1-k_1)\right]F \\ \sigma_{\max} = \left[1+\left(\dfrac{\beta_k}{\beta_\sigma}\right)\coth\beta_k l\right]\beta_\sigma^2 M_k \end{cases} \tag{2.66}$$

where

$$k_1 = (1+\frac{t_a}{t_1})k \tag{2.67}$$

Adhesive stresses shown in Eqs. (2.64) and (2.66) were presented by Goland and Reissner (1944), and then Hart-Smith (1973). Because they are derived on the basis of Fig. 2.4, large deflection effects of the overlap are not included (Tsai and Morton 1994).

In the 2nd analytical framework of the fully-coupled nonlinear analysis, the analytical solutions of the CLS specimen are found for the roller-roller boundary conditions (SLJ) and symmetrical adherends in the existing literatures (Luo and Tong 2007). The simplified analytical solutions for the edge moment factor and the maximum adhesive stresses are:

$$k = \frac{1+(\beta_k c)^2\left[\dfrac{\beta_\tau c f(\beta_{a2}c)-1}{8\beta_\tau c(1+t_a/t_1)}\right]}{1+(\beta_k c)\coth\beta_k l+(\beta_k c)^2\left[\dfrac{1}{2\beta_\sigma c}+\dfrac{\beta_\tau c f(\beta_{a2}c)+3}{8\beta_\tau c}\right]} \tag{2.68}$$

$$\begin{cases} \tau_{\max} = \dfrac{1}{8}\left[(3k_1+1)\beta_{a1}\coth\beta_{a1}c + 3(1-k_1)\beta_{a2}\coth\beta_{a2}c\right]F \\ \sigma_{\max} = \left[1+\left(\dfrac{\beta_k}{\beta_\sigma}\right)\coth\beta_k l\right]\beta_\sigma^2 M_k \end{cases} \tag{2.69}$$

where,

$$f(\beta_{a2}c) = \frac{\beta_{a2}c\coth\beta_{a2}c - 1}{(\beta_{a2}c)^2} \tag{2.70}$$

The analytical solutions based on the fully-coupled nonlinear formulations can also be applied to the symmetrical CLS specimen with other boundary conditions.

By comparing the edge moment factor and the maximum adhesive stresses for the analytical framework of Goland and Reissner (1944) with those based on Luo and Tong (2007), differences of the results can be found in the edge moment factor and the shear stress. It is noted that expressions of the maximum peel stress for the two formulations are the same when the same force boundary conditions are prescribed.

2.3.4 Issues for CLS Joints with Composite Adherends

When the adherends of the CLS specimen are composite laminates, analytical solutions for the CLS are very complicated. Tsai et al. (1998) indicated that the factors such as the inherent material heterogeneity, residual stresses, free-edge effects and relatively low transverse strength and shear stiffness impose great complexity to bonded composite structures.

For the composite laminates widely used in engineering, effects of inherent material heterogeneity, lay-up sequence, lower transverse strength and shear stiffness may be analytically modeled. When the material heterogeneity is considered, the governing equations become the inhomogeneous differential equations, which can also be solved analytically. When the adherends are composite laminates with the symmetrical lay-ups, the formulations presented in this chapter can be extended to the composite CLS specimen; the coefficients α_a and α_k may reflect influences of the lay-ups. By using the Timoshenko beam or higher order theories, the lower transverse stiffness can be modeled and the analytical analysis can also be conducted.

2.4 Influence of Adherend's Large Deflections and Adhesive Deformations

In this section, numerical results of the analytical solutions are presented and compared with the geometrically nonlinear finite element analysis (NFEA) for edge moment factor, overlap deflections and adhesive stresses. The CLS specimen with the roller-roller boundary conditions and the symmetrical adherends are considered and the input data used in this section are: $E_1 = 70\,\text{GPa}$, $\nu_1 = 0.34$ and $t_1 = 1.6\,\text{mm}$; $E_a/E_1 = 0.04$, $t_a/t_1 = 0.078$, $\nu_a = 0.4$; $c/t_1 = 32$ and $l/c = 1.25$. The NFEA results were conducted by Luo and Tong (2007, 2008) using the commercial FEA package MSC/NASTRAN, In the NFEA model, a 4-node isoparametric element was used for both the adhesive and the adherends; 3 and 18 elements were used through the adhesive and adherend thickness in the regions of $0.8c \leq |x| \leq c$, 1 and 6 elements were used in the other region of the overlap. The geometrically nonlinear FEA with plane strain was implemented.

2.4.1 Edge Moment Factor

Figure 2.6 shows the edge moment factor for the CLS with the long overlap. In this figure, NFEA is referred to the NFEA results of MSC/NASTRAN; GR, HS, OP and LT represent the numerical results predicted by Goland and Reissner (1944), Hart-Smith (1973), Oplinger (1994) and Luo and Tong (2007) analytical formulations. These symbols are used in all relevant figures in this chapter.

Figure 2.6 illustrates that the edge moment factor predicted by Hart-Smith (1973) is significantly lower than that predicted by the NFEA, and the predictions of Oplinger (1994), and Goland and Reissner (1944) is obviously higher than the NFEA results. Nevertheless, the edge moment factor predicted by the NFEA and the fully-coupled nonlinear formulation correlates well with each other. It should be noted that Eq. (2.57) is used to calculate k of Goland and Reissner (1944) in Fig. 2.6 for the consistency. More results of comparisons of the fully-coupled nonlinear formulation conducted by Luo and Tong (2007) and the NFEA presented by Tsai and Morton (1994) can be found in Luo and Tong (2007).

As the geometrically nonlinear FEA can properly model behaviors of the geometric nonlinearity, the numerical results of Fig. 2.6 indicate large deflections of the outer adherend and the overlap have to be included in the analytical analysis for the CLS specimen.

It should be pointed out that, the used data ($E_1 = 70\,\text{GPa}$ and $E_a/E_1 = 0.04$) denote the intermediately flexible adhesive (Tsai and Morton 1994). For the flexible adhesive, the difference between the Goland and Reissner (1994) and the NFEA (Tsai and Morton 1994) is larger (see Luo and Tong 2007). That is, the adhesive deformations should also be taken into account in the analytical analysis for the CLS specimen.

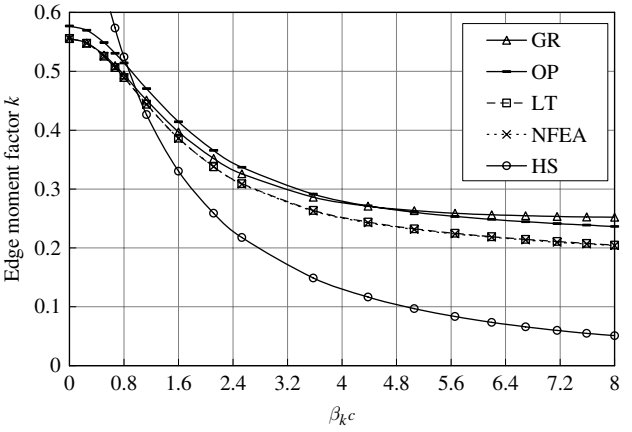

Fig. 2.6 Bending factor predicted by the NFEA and the analytical solutions presented by Goland and Reissner (GR), Hart-Smith (HS), Oplinger (OP), and Luo and Tong (LT) for the CLS specimen with the roller-roller boundary condition

2.4.2 Adherend's Deflections

Figure 2.7 shows the deflection of adherend 1 in the overlap region at $\beta_k c = 8$ predicted by Goland and Reissner (1944), the NFEA and Luo and Tong (2007). It is noted that deflections of adherends 1 and 2 are the same in the Goland and Reissner formulations. The non-dimensional deflection ($w_n = w_1/t_1$) and the non-dimensional overlap axis ($\xi = x/c$) were used in Fig. 2.7.

Figure 2.7 indicates that the overlap deflection predicted by the fully-coupled nonlinear formulations (Luo and Tong 2007) is almost the same as that of the NFEA, but there exist noteworthy difference between the NFEA and the formulations separated in two steps (Goland and Reissner 1944). It is further evident that the adhesive deformations should be considered in the analytical method for the CLS.

2.4.3 Adhesive Stresses

The shear and peel stresses predicted by Goland and Reissner (1994) the NFEA and Luo and Tong (2007) are plotted in Figs. 2.8 and 2.9 respectively. In Figs. 2.8 and 2.9, a beam/adhesive model was used in the analytical analyses. The peak shear and peel stresses occur at the adhesive edge (i.e., crack-tip of the CLS). In the two-dimensional analysis using FEA, the peak shear stress occurs very close to the adhesive edges but shear stress is zero at the edge, while peel stresses at the adhesive edge are singular. Therefore, the stress distributions in Figs. 2.8 and 2.9 are plotted in the range of ($-1 \leq \xi \leq -0.801$) for the present analytical solutions and in the range of ($-0.999 \leq \xi \leq -0.801$) for the NFEA.

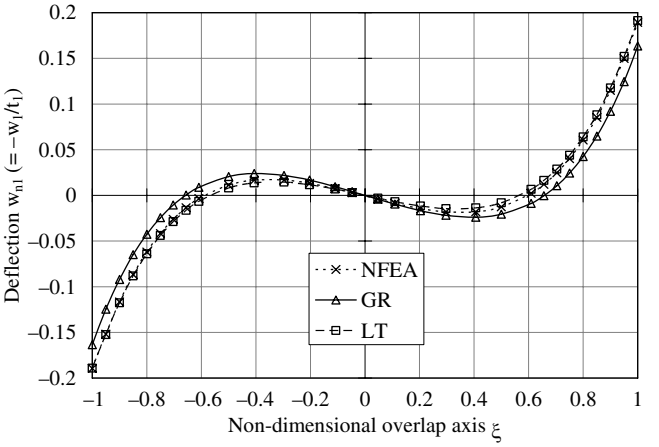

Fig. 2.7 The overlap deflection predicted by the NFEA, Goland and Reissner (GR), and Luo and Tong (LT) formulations for the CLS with the roller-roller boundary condition

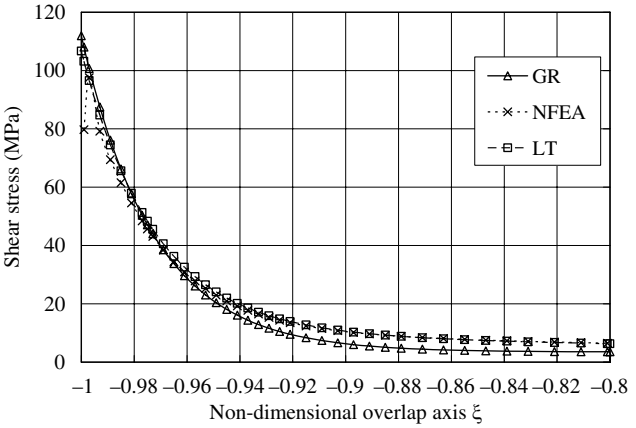

Fig. 2.8 Shear stress predicted by the NFEA, Goland and Reissner (GR), and Luo and Tong (LT) formulations for the CLS with the roller-roller boundary condition

The numerical results in Figs. 2.8 and 2.9 are those at $\beta_k c = 8$, corresponding to a tensile force of 659.6 N/mm. Stresses at the element centre were used in the figures.

Figure 2.8 illustrates the shear distribution predicted by Luo and Tong (2007) correlates better with the NFEA results than that of Goland and Reissner (1944). Even for the same edge moment, there still exists difference between the two formulations for the shear stress prediction, which can also be seen from Eqs. (2.66) and (2.69).

Figure 2.9 is the peel stresses distribution predicted by Goland and Reissner (1944), the NFEA and Luo and Tong (2007). It can also be seen that, as compared to the NFEA, the fully-coupled nonlinear formulations for the peel stress prediction

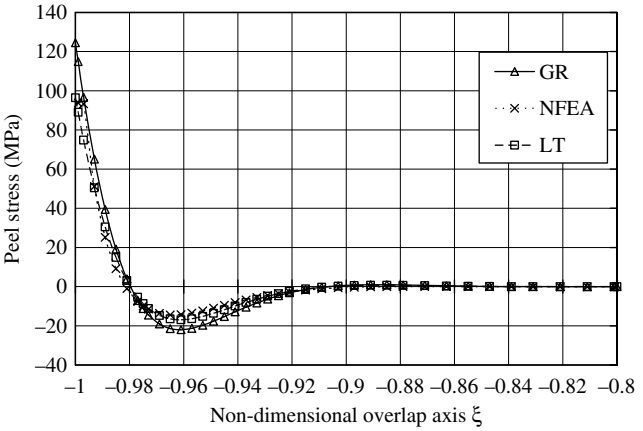

Fig. 2.9 Peel stress predicted by the NFEA, Goland and Reissner (GR), and Luo and Tong (LT) formulations for the CLS with the roller-roller boundary condition

are superior to the formulations separated in two steps based on Goland and Reissner (1944). When the same edge moment is applied, the maximum peel stress predicted by the two formulations is the same.

In the fully-coupled nonlinear formulations (Luo and Tong 2007, 2008), solutions are found for the displacements. In the formulation process, large extensions, large rotations and deformations (material nonlinearity) are neglected. However, the predicted numerical results of edge moment factor, adhesive stresses, adherend deflections correlate extremely well with those of the NFEA. It indicates that large deflections of adherends are the critical feature of the CLS specimen, which is well represented by the fully-coupled nonlinear formulations.

2.5 Strength Prediction

The failure of a CLS specimen may occur in adherend and adhesive and at a bimaterial interface. The failure load may be predicted by the strength-of-material based approach and/or the fracture mechanics based approach (Adams et al. 1997, Tong and Steven 1999), depending on the material properties, adhesive joint configurations and the pre-crack features. A cohesive damage zone model has also attracted attention to predict failure loads of adhesive joints (Sheppard et al. 1998, Yang and Thouless 2001, Blackman et al. 2003, Liljedahl et al. 2006), as there is a cohesive or plastic deformation zone near the crack-tip or the adhesive ends of the CLS specimen generally.

2.5.1 Strength of Material Based Approach

The strength of material based approach involves a stress analysis of the CLS specimen, and employment of stress and/or strain based failure criteria. One of the most widely used stress/strain based failure criteria is the von Mises criterion. It has also been considered for the adhesive joints (Kusenko and Tammzs 1981, Czarnocki and Piekarski 1986), in which the failure criteria on the basis of the tensile experimental testing and biaxial experimental testing have been discussed for maximum tensile stress criterion, maximum tensile strain criterion and the modified distortion energy criterion. Crocombe et al. (1990) addressed structural adhesive failures based on strength of materials and fracture mechanics.

Because of the stress concentration, complexity of stress analysis and difficulty in experimental testing, the strength of material based criteria for predicting the failure criteria based on strength of materials for adhesive joints have not been well-established (Lee 1991, Yang and Thouless 2001). Also, the CLS specimen is mainly designed to test fracture behaviors of the adhesive joints. Mangalgiri and Johnson (1986) discussed the CLS design to ensure the CLS failure occurred in adhesive and interface. Therefore, most of works on the failure prediction for the CLS has been focused on the fracture mechanics based approach.

2.5.2 Calculation of Energy Release Rates and Failure Prediction

The fracture mechanics based approach for the CLS failure prediction includes calculation of the stress intensity factors (SIF) and/or energy release rate (ERR) or J-integral and the experimental testing for the fracture toughness, critical ERRs or J-integral.

When the maximum adhesive stresses are found, energy release rates G_I and G_{II} can be calculated by (Edde and Verreman 1992, Krenk 1992):

$$G_I = \frac{t_a}{2E_a}(\sigma_{\max})^2;\ G_{II} = \frac{t_a}{2G_a}(\tau_{\max})^2 \tag{2.71}$$

It is noted that both modes I and II are found in Eq. (2.71), which can be directly applied to the CLS with relatively long overlap (Krenk 1992).

When the CLS deflections and force components of the overlap are solved, the ERRs and/or the J-integral can be calculated. Lai et al. (1996) calculated the ERRs using the method developed by Hutchinson and Suo (1992) for the bi-material crack. Fernlund and Spelt (1994) calculated J-Integral using the following procedure.

As shown in Fig. 2.10, a closed-form expression of the energy release rate can be calculated by using the J-integral:

$$J = \int_{\Gamma} \left(\boldsymbol{W}\boldsymbol{n} - \boldsymbol{T}\frac{\partial \boldsymbol{u}}{\partial \boldsymbol{\tau}} \right) d\Gamma \tag{2.72}$$

where $\boldsymbol{W}$ is the strain energy density; $\boldsymbol{n}$ and $\boldsymbol{\tau}$ are outward unit normal and tangential vectors to the un-deformed boundary contour; $\boldsymbol{T}$ is the traction vector acting on Γ. When the contour is o–a–b–c–d–e–f–o, no contributions to the J-integral in o–a, b–c, d–e and f–o boundaries as there are no tractions on the crack faces and horizontal boundaries of the upper and lower adherends. The J-integral becomes:

$$J = J_{(1)} + J_{(2)} + J_{(3)} \tag{2.73}$$

where subscripts (1), (2) and (3) represent the boundaries a–b, c–d and e–f respectively. The total energy release rate can be found in light of Eqs. (2.72) and (2.73), which is given by:

$$J = \left(\frac{N_1^2}{2A_{(1)11}} + \frac{M_1^2}{2D_{(1)11}} \right) + \left(\frac{N_2^2}{2A_{(2)11}} + \frac{M_2^2}{2D_{(2)11}} \right) - \left(\frac{N_3^2}{2A_{(o)11}} + \frac{M_3^2}{2D_{(o)11}} \right) \tag{2.74}$$

where subscripts (1), (2) and (o) represent the upper adherend, lower adherend and the overlap. It is noted that Eqs. (2.72), (2.73), (2.74) can be applied to general adhesive joints. For the CLS specimen as shown in Fig. 2.1, $J_{(2)} = 0$. It is also worth noting that the shear force effects on ERRs are not included.

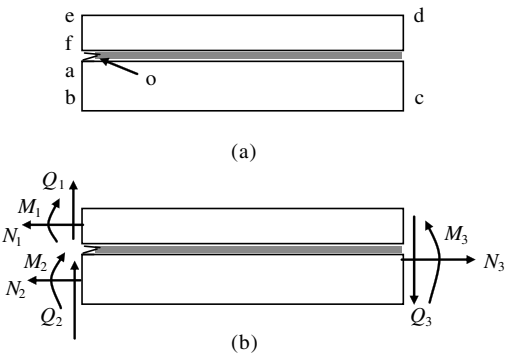

Fig. 2.10 The schematics for J-integral (**a**) the J-integral boundary (**b**) force components of the overlap

When the J-integral of the mixed mode is found, the mode should be separated to predict the CLS failure, because the CLS is generally a mixed mode problem. There exist analytical methods for partitioning modes for a cracked homogeneous beam (e.g., Hutchinson and Suo 1992). For the CLS, the NFEA is an effective tool to calculate mode ratios (Johnson 1986).

Papini et al. (1994), Fernlund and Spelt (1994) conducted the experimental investigation on the critical energy releases rate for the CLS and presented the critical energy release rate for the 7075-T6/Permabond ESP 310 adhesive system, as shown in Fig. 2.11.

When the loading phase angle is found, the critical J-integral J_c can be found from the fracture envelope such as that shown in Fig. 2.11. By comparing the found J-integral J_c with the critical one, the failure loads of the CLS specimens can be predicted.

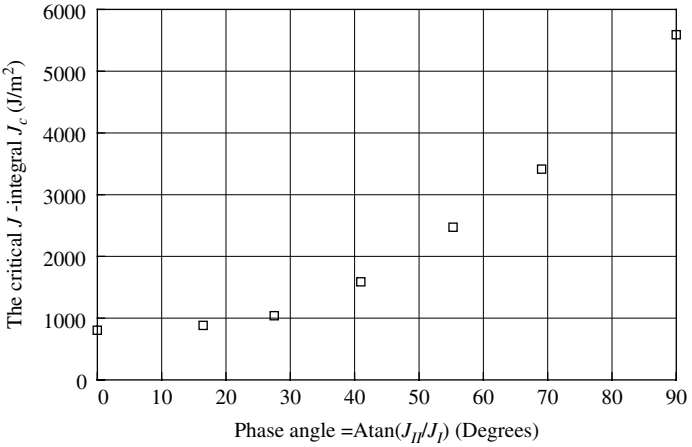

Fig. 2.11 The critical energy release rate of the 7075-T6/Permabond ESP 310 adhesive system

2.6 Concluding Remarks

In this chapter, analytical procedures for stress analysis and failure prediction of the CLS specimen are presented. Because of the complexity, particularly when lap adherend and/or lap adherend of the CLS are composite laminates, closed-form solutions of the CLS are very limited in the existing literatures. Available results show that large deflections of the outer adherend and the overlap must be modeled.

The analytical formulation based on Goland and Reissner (1944) are available to calculate the force components at the end of the overlap, both for symmetrical and asymmetrical adherends, but larger errors may appear as the adhesive deformations are not modeled in the formulations, particularly for the cases of long overlaps, thicker and/or soft adhesive, larger applied loadings and composite laminates. The adhesive stresses of general asymmetrical adherends for the prescribed force boundary conditions can be found in Luo and Tong (2002).

The analytical solution based on the fully-coupled nonlinear formulations (Luo and Tong 2007) correlate well with the geometrically nonlinear finite element analysis; it can also be applied to the composite laminates. Currently, the analytical solutions are only available for the symmetrical adherends. The analytical solutions for CLS with the clamped-clamped and roller-clamped boundary conditions are yet to be found, and that for the CLS with asymmetrical adherends should be further studied.

Acknowledgments The authors are grateful to the continuous support of ARC (Australia) and AOARD/ASOSR (USA).

References

Adams RD, Comyn J, Wake WC (1997) Structural Adhesive Joints in Engineering, Chapman and Hall, London

Alif N, Carlsson LA, Gillespie Jr JW (1997) ASTM STP. 1242:82–106

Benzeggaph ML, Kenane M (1996) Composite Science and Technology. 56:439–449

Blackman BRK, Hadavinvia H, Kinloch AJ, Williams JG (2003) International Journal of Fracture. 119:25–46

Brussat TR., Chiu ST, Mostovoy S (1977), Fracture Mechanics for Structural Adhesive Bonds, AFNLTR-77-163, Air Force Materials Laboratory, Wright-Patterson AFB, Ohio

Carpenter W (1973) International Journal for Numerical Methods in Engineering. 6:450–451

Carpenter W (1980) International Journal for Numerical Methods in Engineering. 15:1659–1680

Cheuk PT, Tong LY (2002) Composites Science and Technology. 62:1079–1095

Crocombe AD, Bigwood DA. Richardson G (1990) International Journal of Adhesion and Adhesives. 10:167–178

Czarnocki P, Piekarski K (1986) International Journal of Adhesion and Adhesives. 6:93–95

Dattaguru B, Everett RA Jr, Whitcomb JD, Johnson WS (1984) Journal of Engineering Materials and Technology-Transactions of the ASME. 106:59–65

Edde F, Verreman Y (1992) International Journal of Adhesion and Adhesives. 12:43–48

Fernlund G, Papini M, McCammond D, Spelt JK (1994) Composites Science and Technology. 51:587–600

Fernlund G, Spelt JK (1991a) International Journal of Adhesion and Adhesives. 11:213–220
Fernlund G, Spelt JK (1991b) International Journal of Adhesion and Adhesives. 11:221–227
Fernlund G, Spelt JK (1994) Composites Science and Technology. 50:441–449
Goland M, Reissner E (1944) Journal of Applied Mechanics. 11:A17–A27
Harbert SJ, Hogan HA (1992) Journal of Reinforced Plastics and Composites. 11:443–457
Hart-Smith LJ (1973) Adhesive-bonded Single-Lap Joints, CR-112235, NASA Langley Research Center
Higgins A (2000) International Journal of Adhesive and Adhesion. 29:367–376
Hutchinson JW, Suo Z (1992) Advance in Applied Mechanics. 29:63–191
Johnson WS (1986) Stress Analysis of the Cracked Lap Shear Specimen: An ASTM Round Robin, NASA Technical Memorandum 89006
Ko TC, Chu RC, Lin CC (1994) Theoretical and Applied Fracture Mechanics. 21:177–195
Krenk S (1992) Engineering Fracture Mechanics. 43:549–559
Kuo AS (1984) AIAA Journal. 22:1460–1464
Kusenko VS, Tammzs VP (1981) Fracture Micromechanics of Polymer Materials, Maritinus Nijhoff Publishers, The Hague/Boston/London
Lai YH, Rakestraw MD, Dillards DA (1996) International Journal of Solids and Structures. 33:1725–1743
Lee LH (1991) Adhesive Bonding, Plenum Press, New York
Liljedahl CDM, Crocombe AD, Wahab MA, Ashcroft IA (2006) International Journal of Fracture. 141:147–161
Lin C, Liechti KM (1987) Journal of Adhesion. 21:1–24
Luo QT, Tong LY (2002) International Journal Solids and Structures. 39:4677–4695
Luo QT, Tong LY (2004) Computational Mechanics. 33:108–120
Luo QT, Tong LY (2007) International Journal of Solids and Structures. 44:2349–2370
Luo QT, Tong LY (2008) International Journal of Adhesion and adhesives, (In Press: DOI: 10.1016/j.ijadhadh.2008.0.007)
Mangalgiri PD, Johnson WS (1986) Journal of Composites Technology and Research. 8:58–60
Oplinger DW (1994) International Journal of Solids and Structures. 31:2565–2587
Panigrahi SK, Pradhan B (2007) Journal of Reinforced Plastics and Composites. 26:183–201
Papini M, Fernlund G, Spelt JK (1994) International Journal of Adhesion and Adhesives. 14:5–13
Rao BN, Acharya AR (1995) Engineering Fracture Mechanics. 51:317–322
Rhee KY (1994) Composite Structures. 29:379–382
Rhee KY, Chi CH (2001) Journal of Composite Materials. 35:77–93
Rhee KY, Ernst HA (1993) Composites Science and Technology. 46:399–405
Rhee KY, Lee SG. Choi NS, Park SJ (2003) Materials Science and Engineering A. 357:270–276
Schmueser DW, Johnson NL (1990) Journal of Adhesion. 32:171–191
Sheppard A, Kelly D, Tong LY (1998) International Journal of Adhesion and Adhesives. 18:385–400
Suo Z, Hutchinson JW (1990) International Journal of Fracture. 43:1–18
Tong LY, Steven GP (1999) Analysis and Design of Structural Bonded Joints, Kluwer Academic, Boston
Tsai MY, Morton J (1994) International Journal of Solids and Structures. 31:2537–2563
Tsai MY, Oplinger DW, Morton J (1998) International Journal of Solids and Structures. 35:1163–1185
Wang H, Vu-Khahn T, Le VN (1995) Journal of Composite Materials. 29:833–849
Wu G, Crocombe AD (1996) Computers and Structures. 61:385–391
Yang C, Sun W, Timblin JS, Stantley SS (2007) Journal of Composite Materials. 41:1579–1602
Yang C, Tomblin JS, Guan Z (2003) Analytical Modeling of ASTM Lap Shear Adhesive Specimens, DOT/FAA/AR-02/130, U.S. Department of Transportation Federal Aviation Administration Office of Aviation Research, Washington, D.C. 20591
Yang MD, Thouless MD (2001) International Journal of Fracture. 110:175–187.

http://www.springer.com/978-3-540-79055-6

Modeling of Adhesively Bonded Joints
da Silva, L.F.M. (Ed.)
2008, X, 335 p., Hardcover
ISBN: 978-3-540-79055-6